Volume 4 | Number 5 | May 2020

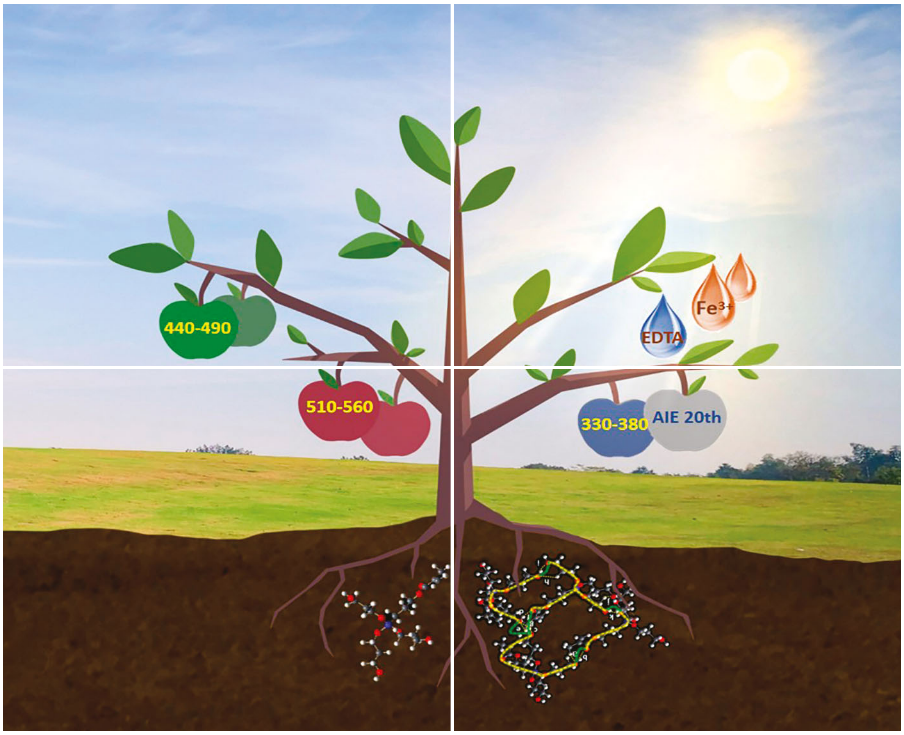

MATERIALS CHEMISTRY FRONTIERS

CCS 中国化学会 CHINESE CHEMICAL SOCIETY
ICCAS
ROYAL SOCIETY OF CHEMISTRY
rsc.li/frontiers-materials

MATERIALS CHEMISTRY
FRONTIERS

RESEARCH ARTICLE

Cite this: *Mater. Chem. Front.*, 2020, 4, 1375

Multiring-induced multicolour emission: hyperbranched polysiloxane with silicon bridge for data encryption†

Yuanbo Feng,[a] Hongxia Yan, *[a] Fan Ding,[a] Tian Bai,[a] Yufeng Nie,[b] Yan Zhao,[a] Weixu Feng *[a] and Ben Zhong Tang *[c]

Received 10th February 2020, Accepted 25th March 2020

DOI: 10.1039/d0qm00075b

rsc.li/frontiers-materials

Multicolour emissive nonconventional macromolecular luminogens with aggregation-induced emission have drawn great attention due to their potential application in a wide range of areas. However, the exploration of efficient synthetic strategies and emission mechanisms still remains a challenge. Herein, we report a facile route to the synthesis of hyperbranched polysiloxane (**P1**) with adjacent –C═O and –C═C groups. Surprisingly, it not only showed blue emission under white light excitation, but also exhibited multicolour luminescence under different excitation wavelengths. Especially, multiple through-space conjugation rings can be found between the first generation **P1** molecules *via* DFT calculation; based on its remarkable luminescence properties, we proposed a new luminescence mechanism namely "multiring-induced multicolour emission" (MIE). In addition, the stimuli-responsive behaviour of **P1** as well as its application in data encryption based on the quenching effect of Fe^{3+} was studied. This work provides guidance to design and synthesise nonconventional macromolecular AIEgens with multicolour luminescence.

1. Introduction

In recent years, nonconventional macromolecular luminogens[1,2] such as polyester,[3] polyethyleneimine (PEI),[4] polyamino esters (PAE),[5] polyurea,[6] and polyamide amine (PAMAM)[7,8] have been extensively researched. The lack of aromatic structures endow these polymers with advantages such as environmental friendliness,[9] good biocompatibility[10] and low toxicity.[11,12] Therefore, they exhibit promising applications in fluorescent probes, cell imaging, biomedicine and so on.[13–16] Normally, the luminescence of nonconventional macromolecular luminogens is explained in terms of the clustering-triggered emission mechanism,[17] which suggests that the luminescence of nonconventional macromolecular luminogens with π and lone-paired (n) electrons can be attributed to the electron cloud overlap and simultaneous conformation rigidification in their aggregated state. Based on this theory, a series of new luminescent materials such as polycarbonate[18] or PAE[19] have been reported. However, the discussion on the luminescence mechanism of these polymers generally stays on the influence of aggregate morphology; in fact, the molecular structure also plays an important role in luminescence performance.

Hyperbranched polysiloxanes (HBPSi), which combine the advantages of both hyperbranched polymers and polysiloxanes, are a promising class of biocompatible luminescent materials. The introduction of the siloxane group to the polymer backbone can not only change their interspace configuration thus affecting their luminescence, but can also be a fine tool to adjust their stability. In our previous work, we have developed various HBPSi and focused on the relationship between their functional groups and luminescence performance. In addition, the application of HBPSi as an air purifier[20] or Fe^{3+} probe[21–24] has also been successfully realized. However, some scientific issues with HBPSi still await further investigation.

Currently, despite the fact that a broad series of HBPSi have been obtained, compared with traditional conjugated luminescent polymers,[25] these HBPSi still have drawbacks such as short and narrow excitation wavelength in the ultraviolet region as well as monochromatic blue emission, which seriously restrict their application. Recently, some non-conjugated luminescent polymers have been reported to exhibit excitation-dependent properties such as poly[(1-octene)-*co*-(itaconic anhydride)],[26] poly(maleic anhydride-*alt*-vinyl acetate)[27] and poly(maleic anhydride-*alt*-vinyl pyrrolidone),[28] which prompted us to design and synthesise novel hyperbranched polysiloxanes with strong and red-shifted

[a] *School of Chemistry and Chemical Engineering, Northwestern Polytechnical University, Xi'an 710072, China. E-mail: hongxiayan@nwpu.edu.cn, fwxdk@nwpu.edu.cn*
[b] *School of Mathematics and Statistics, Northwestern Polytechnical University, Xi'an 7100072, China*
[c] *Department of Chemistry, The Hong Kong University of Science & Technology, Clear Water Bay, Kowloon, Hong Kong, China. E-mail: tangbenz@ust.hk*
† Electronic supplementary information (ESI) available. See DOI: 10.1039/d0qm00075b

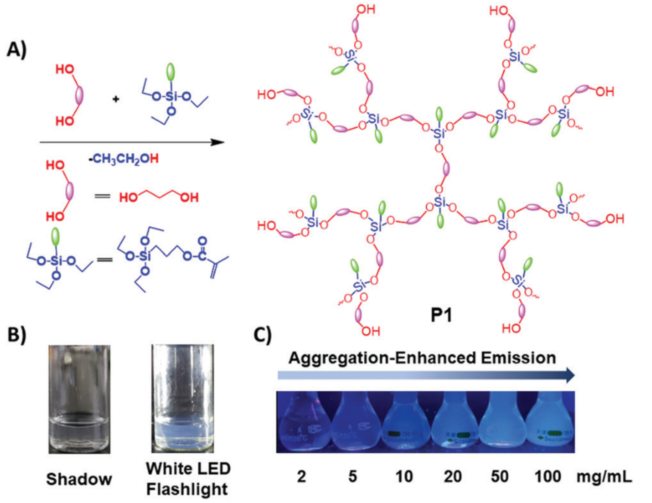

Fig. 1 (A) Synthetic route toward **P1**; (B) 15 mg mL^{-1} **P1** ethanol solution under white LED flashlight or shadow; (C) **P1** ethanol solution with different concentrations under 365 nm UV light.

fluorescence emission. Moreover, it will be also important to expand the HBPSi to novel applications. In this work, we have synthesized a novel HBPSi (**P1**) with adjacent –C═O and –C═C groups (Fig. 1) as well as the reference linear polysiloxane (**P2**, Scheme S1, ESI†) *via* one-step transesterification polycondensation reaction with no catalyst or solvent. Surprisingly, **P1** exhibited multicolour luminescence under different excitation wavelengths. Theoretical calculations, TEM and DLS were employed to study these interesting luminescence properties. Furthermore, the stimuli-responsive behaviour of **P1** was also studied; based on the quenching effect of **P1** due to Fe^{3+}, the application of **P1** in data encryption was also successfully realized.

2. Experimental

The information about starting materials and characterization methods is provided in ESI.†

Synthesis of P1

A mixture of 1,3-propanediol (0.375 mol, 28.54 g) and 3-triethoxysilylpropyl-2-methylprop-2-enoate (MPTS) (0.18 mol, 52.28 g) was stirred in a 250 mL four-necked flask equipped with a mechanical stirrer, a thermograph, an N_2 gas inlet, and a condenser under normal ambient conditions. Then, the mixture was heated to 110 °C, and meanwhile, some distillate was distilled off. Thereafter, the distillation temperature was maintained at about 55 °C to promote the reaction. The mixture was heated up to 165 °C until the distillation temperature dropped to 30 °C and no more distillate came over. Soon after that, the raw product was poured into a vial and was dialyzed in ethanol to remove the products with low molecular weight. Finally, the solution was rotary evaporated at 45 °C and dried at 62 °C under vacuum for 6 h to yield the target oligomer.

For **P1**: ^{1}H NMR (400 MHz, $CDCl_3$) δ 6.05 (s, 1H), 5.50 (s, 1H), 4.07 (m, 5H), 4.05 (m, 6H), 3.91–3.86 (m, 2H), 3.83–3.77 (m, 2H), 3.74 (t, 4H), 3.71–3.60 (m, 6H), 3.37 (s, 4H), 1.89 (s, 4H), 1.75 (m, 6H), 1.17 (m, 9H), 0.65 (m, 3H). ^{13}C NMR (101 MHz, $CDCl_3$) δ 167.55, 136.32, 125.32, 64.61, 61.04, 58.36, 57.98, 34.13, 31.09, 21.93, 18.24, 7.38.

Synthesis of P2

The synthetic procedure for **P2** is similar to that for **P1**, except that 3-(diethoxymethylsilyl)propyl methacrylate (DMPM) (0.27 mol, 70.31 g) was used instead of MPTS.

For **P2**: ^{1}H NMR (400 MHz, $CDCl_3$) δ 6.05 (s, 1H), 4.05 (t, 4H), 3.76 (m, 16H), 3.64 (m, 4H), 1.88 (s, 4H), 1.77–1.64 (m, 9H), 1.17 (m, 26H), 0.66–0.57 (m, 4H). ^{13}C NMR (101 MHz, $CDCl_3$) δ 167.49, 136.39, 125.21, 77.42, 77.30, 77.11, 76.79, 66.96, 66.66, 64.74, 61.32, 58.37, 34.08, 31.24, 22.13, 18.17, 7.37, 6.47.

3. Results and discussion

FT-IR study

As seen in Fig. S1A (ESI†), compared with the peak of –OH from 1,3-propanediol at 3314 cm^{-1}, the peak of –OH from **P1** moves to 3412 cm^{-1} and becomes weaker. Meanwhile, the peaks at 1635 and 1080 cm^{-1} from vinyl and –C═O groups can be found in **P1**. To further determine if the reaction has occurred, the distillate and pure ethanol were also detected by FT-IR. From Fig. S1B (ESI†), we can see that the spectra of the distillate and standard ethanol are almost the same. So it can be concluded that the distillate is ethanol. This evidence indicates that the transesterification polycondensation occurred successfully. Analogously, as shown in Fig. S2 (ESI†), the characteristic absorption peaks of vinyl and –C═O also appear in **P2**. The spectrum of the distillate during the synthesis of **P2** is almost identical to that of pure ethanol. These are important pieces of evidence to indicate the successfully completed polymerization reaction.

^{1}H NMR study

To further determine the structure of the target polymers, the ^{1}H NMR spectra of **P1** and **P2** as well as the raw materials (DMPM, MPTS and 1,3-propanediol) were recorded. As seen in Fig. S3A(b) (ESI†), the proton peaks marked by 2 & 4, 1 & 5 and 3 at about 4.40 ppm, 3.48 ppm and 1.59 ppm belong to H2 & H4 (HO–$\underline{CH_2}$–CH_2–$\underline{CH_2}$–OH), H1 & H5 ($\underline{H}$O–CH_2–CH_2–CH_2–O$\underline{H}$) and H3 (HO–CH_2–$\underline{CH_2}$–CH_2–OH) of 1,3-propanediol respectively. From Fig. S3A(c) (ESI†), the proton peaks related to H10 [–OOC–(CH_3)C═$\underline{CH_2}$], H9 (–Si–CH_2–CH_2–$\underline{CH_2}$–OOC–), H2 & H4 & H6 (CH_3–$\underline{CH_2}$–O–Si–), H11 [–OOC–(CH_3)C═$\underline{CH_2}$], H8 (–Si–CH_2–$\underline{CH_2}$–CH_2–OOC–), H1 & H3 & H5 ($\underline{CH_3}$–CH_2–O–Si–) and H7 (–Si–$\underline{CH_2}$–CH_2–CH_2–OOC–) of MPTS are observed at around 6.07 & 5.52 ppm, 4.09 ppm, 3.79 ppm, 1.91 ppm, 1.76 ppm, 1.19 ppm and 0.66 ppm respectively. As seen in Fig. S3A(a) (ESI†), the proton peaks marked by 8 at about 6.05 & 5.50 ppm are attributed to the [–OOC–C(CH_3)═$\underline{CH_2}$] group. The proton peak marked by 7 at around 4.07 ppm is associated with H7 from the methylene group (–Si–CH_2–CH_2–$\underline{CH_2}$–OOC–). The proton peaks marked by 13 and 4 & 10 & 12, which can be observed at about

3.75 and 3.72 ppm, are respectively from H4 (HO–CH_2–CH_2–$C\underline{H}_2$–O–Si), H10 & H12 (–Si–O–$C\underline{H}_2$–CH_2–$C\underline{H}_2$–O–Si–) and H13 (–Si–O–$C\underline{H}_2$–CH_3). Meanwhile, the proton peaks of H2 (HO–$C\underline{H}_2$–CH_2–CH_2–O–Si) and H1 ($\underline{H}$O–CH_2–CH_2–CH_2–O–Si) marked by 2 and 1 can be observed at about 3.62 and 3.37 ppm. Furthermore, the proton peaks marked by 9, 3 and 11 respectively corresponding to H9 [–OOC–($C\underline{H}_3$)C=CH_2], H3 (HO–CH_2–$C\underline{H}_2$–CH_2–O–Si) and H11 (HO–CH_2–$C\underline{H}_2$–CH_2–OH) can be observed at around 1.75 ppm, 1.73 ppm and 1.71 ppm respectively. It is worth noting that the proton peak associated with hydroxyl groups ($\underline{H}$O–CH_2–CH_2–CH_2–O–Si) from **P1** at about 3.37 ppm is much weaker than that from 1,3-propanediol at around 3.48 ppm. More importantly, the proton peak at 4.40 ppm from H2 & H4 (HO–$C\underline{H}_2$–CH_2–$C\underline{H}_2$–OH) of 1,3-propanediol disappeared in the ^{1}H NMR spectrum of **P1**. Similarly, the ^{1}H NMR spectrum of **P2** is also in agreement with its proposed structure (Fig. S4, ESI†). The results proved that **P1** and **P2** were synthesized successfully.

^{13}C NMR study

^{13}C NMR spectra of the starting materials (1,3-propanediol and MPTS) as well as **P1** can be seen in Fig. S3B(b) (ESI†). In Fig. S3(b) (ESI†), the carbon signals observed at about 58.31 ppm and 35.89 ppm are respectively related to C1 & C2 (HO–$\underline{C}H_2$–CH_2–$\underline{C}H_2$–OH) and C3 (HO–CH_2–$\underline{C}H_2$–CH_2–OH). As seen in Fig. S3B(c) (ESI†), the peaks at about 167.34 ppm, 136.39 ppm, 125.07 ppm, 66.57 ppm, 58.30 ppm, 22.15 ppm, 18.26 ppm, 187.21 ppm and 6.68 ppm are respectively corresponding to C10 (–OO$\underline{C}$–C(CH_3)=CH_2), C12 (–OOC–$\underline{C}$(CH_3)=CH_2), C11 (–OOC–C(CH_3)=$\underline{C}H_2$), C9 (–Si–CH_2–CH_2–$\underline{C}H_2$–OOC–), C2 & C4 & C6 (CH_3–$\underline{C}H_2$–O–Si–), C8 (–Si–CH_2–$\underline{C}H_2$–CH_2–OOC–), C13 (–OOC–($\underline{C}H_3$)C=CH_2), C1 & C3 & C5 ($\underline{C}H_3$–CH_2–O-Si–) and C7 (–Si–$\underline{C}H_2$–CH_2–CH_2–OOC–) of MPTS. As seen in Fig. S3B(a) (ESI†), the carbon peak of C15 from the ester group (–Si–CH_2–CH_2–CH_2–OO$\underline{C}$–) of **P1** can be found at 167.55 ppm. The carbon peaks marked by C16 and C8 at 136.32 ppm and 125.32 ppm are respectively associated with [–OOC–$\underline{C}$(CH_3)=CH_2] and [–OOC–C(CH_3)=$\underline{C}H_2$]. The carbon peak of C7 for (–Si–CH_2–CH_2–$\underline{C}H_2$–OOC–) and C6 for (–Si–CH_2–$\underline{C}H_2$–CH_2–OOC–) can be observed at about 66.48 and 64.61 ppm. The carbon peaks at 61.04 ppm from (–Si–O–$\underline{C}H_2$–CH_3) and at 57.97 ppm from (–O–CH_2–$\underline{C}H_2$–CH_2–OH) or (–O–$\underline{C}H_2$–CH_2–$\underline{C}H_2$–O–) are respectively corresponding to C4, C10 and C12. The carbon peaks at 34.13 and 31.23 are from C11 (–O–CH_2–$\underline{C}H_2$–CH_2–O–) and C3 (–O–CH_2–$\underline{C}H_2$–CH_2–OH) respectively. The carbon peaks at 21.93 ppm, 18.24 ppm, and 7.38 ppm are corresponding to C14 (–O–CH_2–$\underline{C}H_3$), C6 & C9 (–OOC–C($\underline{C}H_3$)=CH_2) or (–OOC–C($\underline{C}H_3$)=CH_2) and C5 (–Si–$\underline{C}H_2$–CH_2–CH_2–OOC–). In addition, the ^{13}C NMR spectrum of **P2** is also in agreement with its proposed structure (Fig. S5, ESI†). The results proved that **P1** and **P2** were synthesized successfully.

GPC study

The GPC data for **P1–P2** are shown in Fig. S6 and Table S1 (ESI†). **P1** has a broad molecular distribution (PDI = 11.55). Meanwhile, the weight average molecular weight (M_w) of **P1** is 117 700, while its number average molecular weight (M_n) is 10 100. In addition, **P2** has a narrow molecular distribution (PDI = 1.81). The M_w and M_n for **P2** are 11 100 and 20 200, respectively.

Photophysical study

The photophysical properties of **P1–P2** were carefully analysed. As seen in Fig. 1C, when the concentration of **P1** increased from 2 mg mL^{-1} to 100 mg mL^{-1}, its fluorescence under 365 nm UV light gradually enhanced, which shows a typical aggregation enhanced emission (AEE).[29] To our surprise, **P1** ethanol solution (15 mg mL^{-1}) can be excited by a white LED flashlight and showed weak blue luminescence (Fig. 1B). In order to understand this interesting phenomenon, first of all, we systematically studied the UV-vis absorption and PL spectra of **P1**. As observed in Fig. 2A, the UV-vis absorption of **P1** increased with the increase in its concentration from 0.25 mg mL^{-1} to 5 mg mL^{-1}. Due to the small distances between the carbonyl groups, hydroxyl groups and the carbon carbon double bonds of **P1**, there is a strong absorption peak at 220 nm (peak 2), which is corresponding to π–π* electronic transitions. Moreover, peak 1 at 210 nm can be attributed to n–π* electronic transitions. Meanwhile, the absorption peaks showed obvious red shift as the concentration of **P1** increased. This phenomenon could be because of the newly formed "electronic delocalization system"[30] between the silicon and oxygen atoms. It is worth noting that there exists some weak absorption after 300 nm in the UV-vis spectra of the **P1** concentrated solution; however, the peaks around 200–250 nm are too strong and exceed the detection limit, and due to the great difference of intensity between different peaks, it is difficult to see the absorption after 300 nm in Fig. 2A. Subsequently, from the excitation spectra of **P1** (Fig. 2B), we can see that it has a broad excitation range from around 250 nm to 400 nm, especially when at a high concentration; the shoulder peak at around 301 nm remains strong compared with the hyperbranched poly(amino ester)s we synthesized previously,[19] which could be ascribed to the Si–O coordination bonds formed in **P1** ethanol solution at high concentration. In addition, there are also two emission peaks at 410 nm and 435 nm, which may be due to the huge heterogeneity and broad molecular distribution of **P1**.

Moreover, the fluorescence intensity of **P1** increased as its concentration increased from 2 mg mL^{-1} to 100 mg mL^{-1}, consistent with Fig. 1C and also showing a typical aggregation enhanced emission. Finally, we explored the effect of temperature

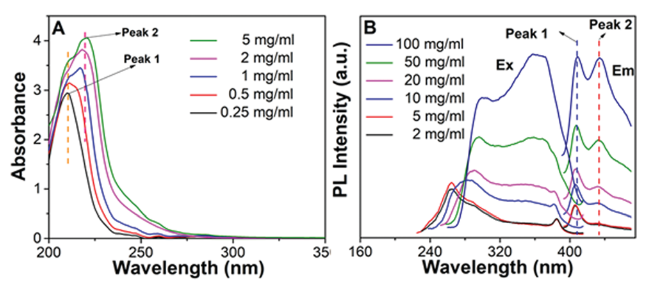

Fig. 2 (A) UV-vis absorption spectra of **P1** ethanol solution with the concentration increased from 0.25 mg mL^{-1} to 5 mg mL^{-1}; (B) excitation (λ_{em} = 406 nm) and emission (λ_{ex} = 360 nm) spectra of **P1** ethanol solution with the concentration increased from 2 mg mL^{-1} to 100 mg mL^{-1}.

on the luminescence of **P1**; as seen in Fig. S7 (ESI†), the luminescence intensity of **P1** increased with the decrease of temperature. The reason for this phenomenon is with the change of concentration or temperature, the movement of polymer chains can be restricted, then less energy will be dissipated by the non-radiative channel leading to the stronger emission. Above all, the broad excitation range and long excitation wavelength of **P1** could be the reason why it can be excited by the white light. To get more insights into the luminescence mechanism of **P1**, we also synthesized the reference linear polymer **P2** for comparison; it is clear that the luminescence intensity and UV-vis absorption of the reference linear polymer **P2** are much lower compared with that of **P1** (Fig. S15 and S16B, ESI†). In addition, as seen in Fig. S17A–D (ESI†), the absolute quantum yields of **P1** and **P2** are 7.71% and 1.12% and their luminescence lifetimes are 1.0 ns and 0.57 ns respectively, which suggests that the hyperbranched structure is crucial for the strong emission when the components of the polymer chains are the same. More interestingly, **P1** exhibits multicolour luminescence at different excitation wavelengths of 330–380 nm, 440–490 nm and 510–560 nm respectively (Fig. 3), which inspires us to further study its multicolour luminescence properties. As seen in Fig. S9 and S14 (ESI†), the emission colour of **P1** (ethanol solution, 100 mg mL^{-1}) changes from deep blue to red with the excitation wavelength increased from 330 nm to 450 nm. In contrast, the reference linear polymer **P2** only emits weak blue fluorescence at the excitation wavelength between 330 and 380 nm, and no multicolour luminescence was detected. These results prove that the synergy of "silicon induced aggregation",[31] the interactions between the adjacent –C=O, –C=C and –OH groups[32] in the hyperbranched topology structure, together with the through-space electronic communication[33,34] may lead to the multiple transition modes such as n–π* or π–π*, enabling the multicolour luminescence property of **P1**.

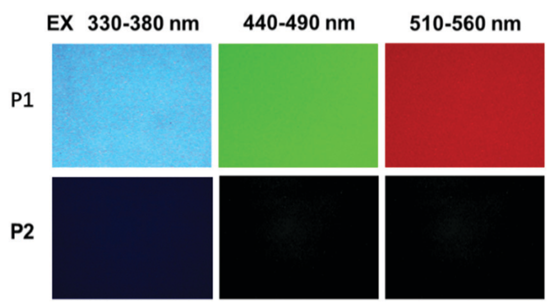

Fig. 3 Fluorescence microscope images of pure **P1** and **P2** under the light filter of UV-2A (Ex 330–380 nm, DM 400, BA 420), B-2A (Ex 440–490 nm, DM 505, BA 520) or G-2A (Ex 510–560 nm, DM 575, BA 590) of **P1**.

In order to theoretically understand the multicolour luminescence mechanism of **P1**, we used the density functional theory (DFT) to determine its energy levels. The first generation molecules of **P1** with the molecule number increased from one to four were examined to simplify the calculation; with the number of molecules increased, the calculated structures become closer. It is obvious that the molecules are aggregated to form a supramolecular hyperbranched structure *via* hydrogen bonds and strong intermolecular interactions (Fig. 4A, B and Fig. S10, ESI†), which may be due to the fact that the Si→O coordination bond (silicon bridge)[35] is flexible and has similar properties to double bonds;[36] it decreases the distances between the chromophores such as –C=O, –OH as well as –C=C groups, helps to form the coplanar through-space conjugation rings of different sizes, promotes the through-space electronic communication and leads to the lower HOMO–LUMO energy levels of **P1** (Table 1). Interestingly, multiring through space conjugation was found in the aggregates of **P1** (Fig. 4A), different from HBPSi which exhibits a high luminescence quantum yield and monochromatic blue emission with single ring through-space conjugation (Fig. S13, ESI†),[37] **P1** exhibits multicolour luminescence though it shows a lower quantum yield. It gives us an idea that the number and size of the conjugation ring as well as its planarity may be related to the luminescence property. Therefore, we made a detailed analysis and comparison between the calculation results from **P1** and our previous works. For HBPSi (Fig. S13, ESI†),[37] on the one hand, the conjugated segments (O=C, Si→O, –C=C) connected by the silicon bridge may form the single ring through-space conjugation and enable its monochromatic blue emission, and on the other hand, the single conjugation ring with high planarity may lead to its high luminescence quantum yield, which agrees well with the traditional luminescence mechanism. Alternatively, as for **P1** (Fig. 4A), the

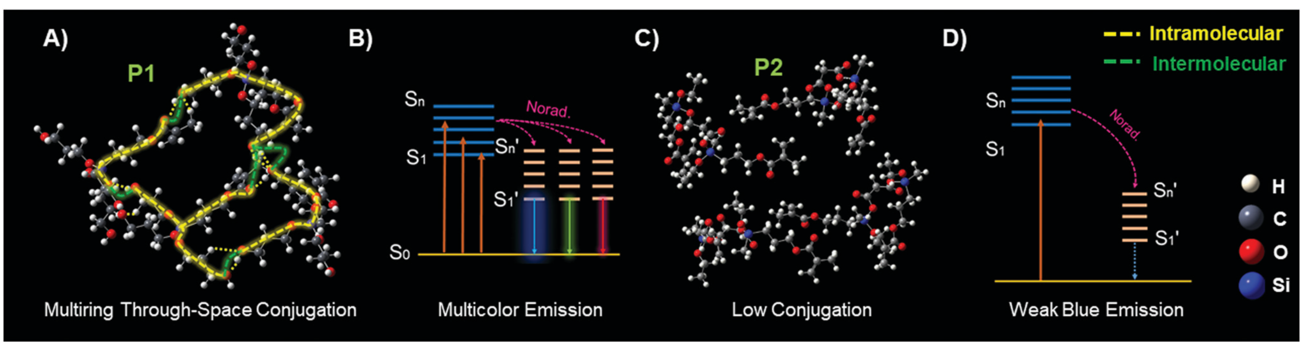

Fig. 4 (A) The accumulation of four **P1** first generation molecules and the "silicon-bridge" promoted multiring through-space conjugation as well as (B) schematic diagram of its luminescence mechanism; (C) the accumulation of four **P2** first generation molecules as well as (D) schematic diagram of its luminescence mechanism.

Table 1 DFT calculation results of the first generation **P1** molecules

Molecule number	E(HOMO)/a.u.	E(LUMO)/a.u.	Energy gap/a.u.	Energy gap/eV
1	−0.263	−0.033	0.230	6.253
2	−0.262	−0.034	0.228	6.214
3	−0.258	−0.032	0.225	6.128
4	−0.237	−0.053	0.184	5.018

multiring through-space conjugation may lead to the different electron delocalization and enable its multicolour luminescence under different excitation wavelengths, and thus, the long wavelength emission may be due to the big conjugation ring. This mechanism can be simply concluded as "multiring-induced multicolour emission" (MIE), and it is also worth noting that the MIE mechanism is applicable to our previous works;[19,38] similar coplanar multiring through-space conjugation can also be found in the aggregates of multicolour luminescent hyperbranched poly(amino ester)s based on the results of DFT calculations (Fig. S12, ESI†). Conversely, due to the linear structure features, it is more difficult for P2 to form strong through space conjugation than **P1** and it has a looser structure (Fig. 4C), and in addition there is no apparent conjugation ring detected, and thus it has a big HOMO–LUMO energy gap (Table S2, ESI†), relatively low luminescence quantum yield and single weak blue emission (Fig. 4D). Then we used the TD-DFT calculations based on the optimized ground geometries to investigate the oscillator strength of the first generation **P1** and **P2** molecules. As seen in Fig. S16A (ESI†), the trend of the calculated UV-vis spectra of **P1** and **P2** is almost the same as their experimental data (Fig. S16B, ESI†). Furthermore, the oscillator strength of **P1** is stronger than that of **P2** (Table S2, ESI†), which means **P1** consumes less excitation energy through the nonradiative channel, and thus it has an excellent luminescence performance.

Subsequently, TEM and DLS were used to verify the proposed luminescence mechanism of **P1**; we analysed the micro-structure morphology of **P1–P2** at different concentrations in ethanol solution. As shown in Fig. 5A, there are only loose structures in 5 mg mL^{-1} **P1** ethanol solution; the polymer chains can vibrate and rotate freely at this concentration, and thus, most of the excitation energy will be consumed *via* the non-radiative transition process. However, as the concentration of **P1** increased to 50 mg mL^{-1}, it assembled into tighter spherical supramolecular polymers (Fig. 5B); then, most of the excitation energy will be converted into luminescence *via* the radiative transition process. Moreover, from the results of DLS (Fig. S8 and Table S3, ESI†), we can see that when the concentration of **P1** increases from 2 mg mL^{-1} to 20 mg mL^{-1}, the main size of the particles is reduced (from 297.4 nm to 13.02 nm). However, when the concentration continues to increase from 20 mg mL^{-1} to 100 mg mL^{-1}, the main size of the particles increases gradually (from 13.02 nm to 20.06 nm) and there are more assemblies with different sizes. The reason for this phenomenon is first of all, the aggregates of **P1** would gradually become more compact when the concentration increases from 2 mg mL^{-1} to 10 mg mL^{-1}, so the main size is reduced. However, due to the space constraints, the particle size may slowly increase as the concentration continues to increase. Meanwhile, as the concentration increases further, there would be more assemblies with different particle sizes. The results of DLS and TEM are consistent with our previous theoretical calculations.

In order to further study the stimuli-responsive behaviour of **P1**, we analysed the fluorescence intensity of **P1** (15 mg mL^{-1}, 1 : 9 water–ethanol solution) in the presence of different metal ions (Ba^{2+}, Na^{+}, Ca^{2+}, Hg^{2+}, Cd^{2+}, Al^{3+}, Fe^{3+}, Cu^{2+}, Zn^{2+}, Co^{2+}). From Fig. 6 and Fig. S18A (ESI†), it is obvious that the luminescence of **P1** can be quenched the most by Fe^{3+} compared with other metal ions ($\Delta I = I_0 - I$; I_0 is the emission intensity of **P1** in water–ethanol solution with different ions). Meanwhile, the relationship between ΔI and the concentration of Fe^{3+} was also studied, and the results showed that there is a linear relationship between the luminescence intensity of **P1** and the concentration of Fe^{3+} ions (1 to 1000 μmol L^{-1}, Fig. S18B, ESI†); the reason for this phenomenon could be that with the formation of **P1**–Fe^{3+}, there is intermolecular charge transfer from Fe^{3+} to **P1** due to the large charge radius ratio of Fe^{3+}. Then we further verified the quenching mechanism by using the strong metal-complexing agent Na_2EDTA, which can coordinate with

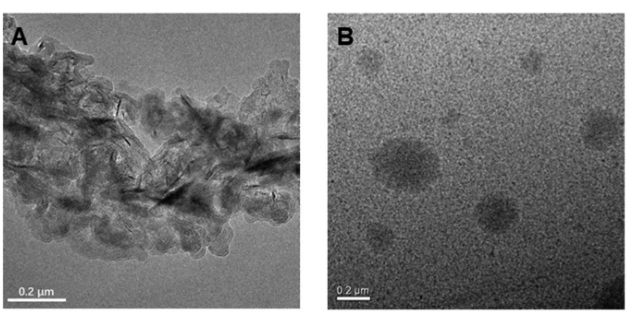

Fig. 5 TEM micrographs of self-assembled morphology of **P1** in ethanol with the concentration at (A) 5 mg mL^{-1} and (B) 50 mg mL^{-1}.

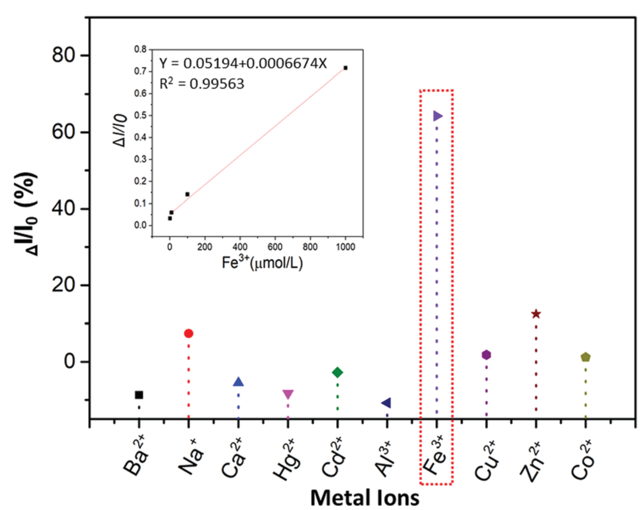

Fig. 6 Luminescence quenching rate ($\Delta I/I_0$) of the 15 mg mL^{-1} **P1** water–ethanol solution with different metal ions (1 × 10^{-3} mol L^{-1}), and the relationship between $\Delta I/I_0$ and the concentration of Fe^{3+}.

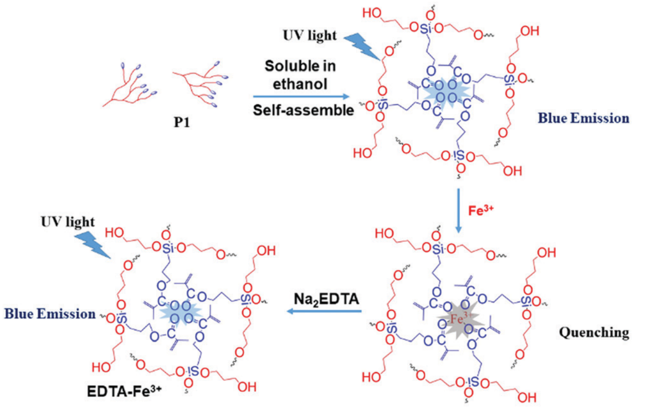

Fig. 7 The mechanism of **P1** as a Fe^{3+} probe: "turn off" (fluorescence quenching after the formation of the **P1**–Fe^{3+} complex); "turn on" (fluorescence restored after the formation of the EDTA–Fe^{3+} complex and the breaking of the **P1**–Fe^{3+} complex).

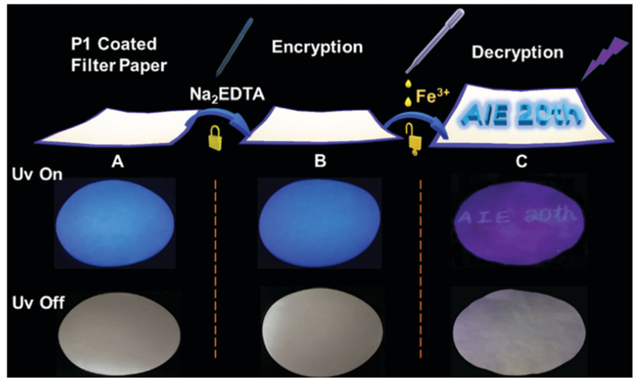

Fig. 8 Photographs of (A) **P1** coated security paper; (B) security paper after writing with Na_2EDTA; (C) security paper treated with $FeCl_3$ (1×10^{-3} mol L^{-1} water–ethanol solution) under natural light or under the irradiation of 365 nm UV light.

Fe^{3+} ions and destroy the structure of **P1**–Fe^{3+}. As shown in Fig. S18C (ESI†), on adding Na_2EDTA into the **P1**–Fe^{3+} solution, the fluorescence intensity of **P1**–Fe^{3+} gradually enhances, which proves the key role of Fe^{3+} in the luminescence quenching of **P1** (Fig. 7). Subsequently, we also explored the solvent effect and pH dependency of **P1** to further comprehend its luminescence mechanism. As seen in Fig. S19A (ESI†), **P1** shows different fluorescence intensity in solvents with different polarity including *N*,*N*-dimethylformamide (DMF), ethanol (EtOH), tetrahydrofuran (THF), *N*-methyl-2-pyrrolidone (NMP) and dimethyl sulfoxide (DMSO). The luminescence intensity decreases with the increase of the solvent polarity. The reason is that **P1** self-assembles into a tighter structure in poor polarity solvents; therefore, it is difficult for the polymer chains to move freely, which causes the stronger fluorescence. From Fig. S19B (ESI†), the luminescence intensity of **P1** is lower under acidic (pH = 2.1, 3.5) or alkaline (pH = 8.5, 9.3) conditions; meanwhile, the luminescence intensity under neutral conditions (pH = 6.8) is the strongest compared to that in other pH conditions. This surprising phenomenon can be attributed to the fact that the intermolecular forces and hydrogen bonds can be destroyed by H^+ or OH^-, thus changing the aggregation morphology of **P1**.

Finally, based on the quenching effect of **P1** due to Fe^{3+}, the application of **P1** in data encryption was realized. First of all, a security paper was fabricated by coating **P1** on a filter paper, which makes the security paper blue luminescent under 365 nm UV light (Fig. 8A). Subsequently, a transparent water solution of Na_2EDTA (15 mg mL^{-1}) was firstly exploited as the ink, by which ''AIE 20th'' was written on the security paper. It was impossible to detect the information by the naked eye under daylight or UV irradiation (Fig. 8B), and thus the information was successfully encrypted. However, after painting a small amount of $FeCl_3$ (1×10^{-3} mol L^{-1} water solution) on the security paper, the sentence appeared with a blue emission under 365 nm UV light (Fig. 8C). This is due to Na_2EDTA protecting the luminescence of **P1** on the security paper from quenching by Fe^{3+} ions; in other words, $FeCl_3$ can be used as a "key" to decode the encrypted information on the security paper. Thus, hyperbranched polysiloxane (**P1**) can be used as a convenient tool to turn the normal paper into security paper for data encryption without changing its appearance.

4. Conclusions

In summary, a novel hyperbranched polysiloxane (**P1**) with multicolour luminescence has been successfully synthesized. Photoluminescence study on **P1** and the linear polymer **P2** showed that the hyperbranched topology structure plays a key role in the luminescence property of **P1**; especially its multicolour luminescence could be ascribed to the multi hydrogen bonds promoted coplanar multiring through-space conjugation according to the results of DFT calculation. This mechanism can be concluded to be ''multiring-induced multicolour emission'' (MIE). In addition, **P1** exhibited luminescence quenching *via* Fe^{3+}, acid base and high polarity solvent stimulation. Furthermore, **P1** can serve as a powerful tool to convert normal paper into security paper without changing its appearance; by using Na_2EDTA as the ink, the information encrypted on the security paper was easily decoded *via* Fe^{3+} stimulation under 365 nm UV light. This work not only provides guidance to the design of nonconventional macromolecular AIEgens with multicolour luminescence, but also expands their application to data security protection.

Conflicts of interest

The authors declare that they have no conflict of interest.

Acknowledgements

This work was funded by the National Natural Science Foundation of China (21875188), Open Fund of Guangdong Provincial Key Laboratory of Luminescence from Molecular Aggregates, Guangzhou 510640, China (South China University of Technology) (2019B030301003), the Fundamental Research Fund for the Central Universities (G2018KY0308), and Key Research and Development Program of Shaanxi (2019ZDLGY04-08).

Notes and references

1 T. Huang, Z. Y. Wang, A. J. Qin, J. Z. Sun and B. Z. Tang, Luminescent polymers containing unconventional chromophores, *Acta Chim. Sin.*, 2013, **71**, 979–990.

2 J. O. Mueller, D. Voll, F. G. Schmidt, G. Delaittre and C. Barner-Kowollik, Fluorescent polymers from non-fluorescent photoreactive monomers, *Chem. Commun.*, 2014, **50**, 15681–15684.

3 Y. Q. Du, H. X. Yan, W. Huang, F. Chai and S. Niu, Unanticipated strong blue photoluminescence from fully biobased aliphatic hyperbranched polyesters, *ACS Sustainable Chem. Eng.*, 2017, **5**, 6139–6147.

4 L. Pastor Pérez, Y. Chen, Z. Shen, A. Lahoz and S. E. Stiriba, Unprecedented blue intrinsic photoluminescence from hyperbranched and linear polyethylenimines: polymer architectures and pH-effects, *Macromol. Rapid Commun.*, 2007, **28**, 1404–1409.

5 D. C. Wu, Y. Liu, C. B. He and S. H. Goh, Blue photoluminescence from hyperbranched poly(amino ester)s, *Macromolecules*, 2005, **38**, 9906–9909.

6 R. B. Restani, P. I. Morgado, M. P. Ribeiro, I. J. Correia, A. Aguiar-Ricardo and V. D. Bonifácio, Biocompatible polyurea dendrimers with pH-dependent fluorescence, *Angew. Chem., Int. Ed.*, 2012, **51**, 5162–5165.

7 J. F. Huang, H. M. Luo, C. D. Liang, I. W. Sun, G. A. Baker and S. Dai, Hydrophobic Brønsted acid–base ionic liquids based on PAMAM dendrimers with high proton conductivity and blue photoluminescence, *J. Am. Chem. Soc.*, 2005, **127**, 12784–12785.

8 H. Lu, L. Feng, S. Li, J. Zhang, H. Lu and S. Feng, Unexpected strong blue photoluminescence produced from the aggregation of unconventional chromophores in novel siloxane–poly(amidoamine) dendrimers, *Macromolecules*, 2015, **48**, 476–482.

9 D. A. Tomalia, B. Klajnert-Maculewicz, A. M. Johnson, H. F. Brinkman, A. Janaszewska and D. M. Hedstrand, Non-traditional intrinsic luminescence: inexplicable blue fluorescence observed for dendrimers, macromolecules and small molecular structures lacking traditional/conventional luminophores, *Prog. Polym. Sci.*, 2019, **90**, 35–117.

10 H. K. Zhang, Z. Zhao and P. R. McGonigal, *et al.*, Clusterization-triggered emission: uncommon luminescence from common materials, *Mater. Today*, 2020, **32**, 275–292.

11 Q. Zhou, B. Cao, C. Zhu, S. Xu, Y. Gong, W. Z. Yuan and Y. Zhang, Clustering-triggered emission of nonconjugated polyacrylonitrile, *Small*, 2016, **12**, 6586–6592.

12 Y. J. Tsai, C. C. Hu, C. C. Chu and I. Toyoko, Intrinsically fluorescent PAMAM dendrimer as gene carrier and nanoprobe for nucleic acids delivery: bioimaging and transfection study, *Biomacromolecules*, 2011, **12**, 4283–4290.

13 L. H. Bai, H. X. Yan, Y. B. Feng, W. X. Feng and L. Y. Yuan, Multi-excitation and single color emission carbon dots doped with silicon and nitrogen: Synthesis, emission mechanism, Fe^{3+} probe and cell imaging, *Chem. Eng. J.*, 2019, **373**, 963–972.

14 R. Ye, Y. Liu, H. Zhang, H. Su, Y. Zhang, L. Xu, R. Hu, R. T. K. Kwok, K. S. Wong and J. W. Y. Lam, W. A Goddrad and B. Z. Tang, Non-conventional fluorescent biogenic and synthetic polymers without aromatic rings, *Polym. Chem.*, 2017, **8**, 1722–1727.

15 L. H. Bai, H. X. Yan, T. Bai, Y. B. Feng, Y. Zhao, Y. Ji, W. X. Feng, T. L. Lu and Y. F. Nie, High fluorescent hyperbranched polysiloxane containing β-cyclodextrin for cell imaging and drug delivery, *Biomacromolecules*, 2019, **20**, 4230–4240.

16 B. Liu, Ya. L. Wang, W. Bai, J. T. Xu, Z. K. Xu, K. Yang, Y. Z. Yang, X. H. Zhang and B. Y. Du, Fluorescent linear CO_2-derived poly(hydroxyurethane) for cool white LED, *J. Mater. Chem. C*, 2017, **5**, 4892–4898.

17 Y. Z. Wang, B. Xin, X. H. Chen, S. Y. Zheng, Y. M. Zhang and W. Z. Yuan, Emission and emissive mechanism of nonaromatic oxygen clusters, *Macromol. Rapid Commun.*, 2018, **39**, 1800528.

18 W. Huang, H. X. Yan, S. Niu, Y. Q. Du and L. Y. Yuan, Unprecedented strong blue photoluminescence from hyperbranched polycarbonate: from its fluorescence mechanism to applications, *J. Polym. Sci., Part A: Polym. Chem.*, 2017, **55**, 3690–3696.

19 L. Y. Yuan, H. X. Yan, L. H. Bai, T. Bai, Y. Zhao, L. L. Wang and Y. B. Feng, Unprecedented multicolor photoluminescence from hyperbranched poly(amino ester)s, *Macromol. Rapid Commun.*, 2019, **40**, 1800658.

20 S. Niu and H. X. Yan, Novel silicone-based polymer containing active methylene designed for the removal of indoor formaldehyde, *J. Hazard. Mater.*, 2015, **287**, 259–267.

21 S. Niu, H. X. Yan, Z. Y. Chen, S. Li, P. L. Xu and X. L. Zhi, Unanticipated bright blue fluorescence produced from novel hyperbranched polysiloxanes carrying unconjugated carbon–carbon double bonds and hydroxyl groups, *Polym. Chem.*, 2016, **7**, 3747–3755.

22 S. Niu, H. X. Yan, Z. Y. Chen, L. Y. Yuan, T. Y. Liu and C. Liu, Water-soluble blue fluorescence-emitting hyperbranched polysiloxanes simultaneously containing hydroxyl and primary amine groups, *Macromol. Rapid Commun.*, 2016, **37**, 136–142.

23 S. Niu, H. X. Yan, S. Li, P. L. Xu, X. L. Zhi and T. T. Li, Bright blue photoluminescence emitted from the novel hyperbranched polysiloxane-containing unconventional chromogens, *Macromol. Chem. Phys.*, 2016, **217**, 1185–1190.

24 S. Niu, H. X. Yan, S. Li, C. Tang, Z. Y. Chen, X. L. Zhi and P. L. Xu, A multifunctional silicon-containing hyperbranched epoxy: controlled synthesis, toughening bismaleimide and fluorescent properties, *J. Mater. Chem. C*, 2016, **4**, 6881–6893.

25 J. Liu, Y. Zhong, J. W. Y. Lam, L. Ping, Y. Hong, Y. Yong, Y. Yue, M. Faisal, H. H. Y. Sung and I. D. Williams, Hyperbranched conjugated polysiloles: synthesis, structure, aggregation-enhanced emission, multicolor fluorescent photopatterning, and superamplified detection of explosives, *Macromolecules*, 2010, **43**, 4921–4936.

26 C. Shang, Y. X. Zhao, N. Wei, H. M. Zhuo, Y. M. Shao and H. L. Wang, Enhancing Photoluminescence of Nonconventional Luminescent Polymers by Increasing Chain Flexibility, *Macromol. Chem. Phys.*, 2019, **220**, 1900324.

27 C. X. Hu, Z. Y. Guo, Y. Ru, W. B. Song, Z. J. Liu, X. H. Zhang and J. L. Qiao, A New Family of Photoluminescent Polymers with Dual Chromophores, *Macromol. Rapid Commun.*, 2018, 1800035.

28 C. Shang, N. Wei, H. M. Zhuo, Y. M. Shao, Q. Zhang, Z. X. Zhang and H. L. Wang, Highly emissive poly(maleic anhydride-*alt*-vinyl pyrrolidone) with molecular weight-dependent and excitation-dependent fluorescence, *J. Mater. Chem. C*, 2017, **5**, 8082–8090.
29 A. J. Qin, J. W. Y. Lam and B. Z. Tang, Luminogenic polymers with aggregation-induced emission characteristics, *Prog. Polym. Sci.*, 2012, **37**, 182–209.
30 W. Z. Yuan and Y. M. Zhang, Nonconventional macromolecular luminogens with aggregation-induced emission characteristics, *J. Polym. Sci., Part A: Polym. Chem.*, 2017, **55**, 560–574.
31 H. Lu, Z. Q. Hu and S. Y. Feng, Nonconventional luminescence enhanced by silicone-induced aggregation, *Chem. – Asian J.*, 2017, **12**, 1213–1217.
32 Z. J. Qiu, X. L. Liu, J. W. Y. Lam and B. Z. Tang, The marriage of aggregation-induced emission with polymer science, *Macromol. Rapid Commun.*, 2019, **40**, 1800568.
33 X. H. Chen, X. D. Liu, J. L. Lei, L. Xu, Z. H. Zhao, F. Kausar, X. Y. Xie, X. Y. Zhu, Y. M. Zhang and W. Z. Yuan, Synthesis, clustering-triggered emission, explosive detection and cell imaging of nonaromatic polyurethanes, *Mol. Syst. Des. Eng.*, 2018, **3**, 364–375.
34 Q. Wang, X. Y. Dou, X. H. Cheng, Z. H. Zhao, S. Wang, Y. Z. Wang, K. Y. Sui, Y. Q. Tian, Y. Y. Gong, Y. M. Zhang and W. Z. Yuan, Reevaluating protein photoluminescence: remarkable visible luminescence upon concentration and Insight into the emission mechanism, *Angew. Chem., Int. Ed.*, 2019, **58**, 2–9.
35 T. Bai, H. X. Yan and S. Niu, *et al.*, Study on structure and luminescence properties of polysiloxane with aggregation-induced emission, *Polym. Bull.*, 2019, **10**, 1–9.
36 Y. N. Shu and B. G. Levine, Do excited silicon–oxygen double bonds emit light?, *J. Phys. Chem. C*, 2014, **118**, 7669–7677.
37 Y. B. Feng, T. Bai, H. X. Yan, F. Ding, L. H. Bai and W. X. Feng, High fluorescence quantum yield based on the through-space conjugation of hyperbranched polysiloxane, *Macromolecules*, 2019, **52**, 3075–3082.
38 Y. Q. Du, T. Bai, H. X. Yan, Y. Zhao, W. X. Feng and W. Q. Li, A simple and convenient route to synthesize novel hyperbranched Poly(amine ester) with multicolored fluorescence, *Polymer*, 2019, **185**, 121771.

